

Re-evaluating photoluminescent defects in Cu_2O

A. Brewin, M.P.A. Jones, S.J. Clark

February 16, 2026

Abstract

Cuprous oxide (Cu_2O) is of interest for several technologies, including solar cells, and more recently, quantum devices via Rydberg excitons. Its performance in these capacities is strongly affected by defects in the crystal. The current best diagnostic for the presence of defects in a sample is the photoluminescence (PL) spectrum, which shows a number of strong lines at energies below the band gap, with brightnesses dependent on the sample. However, the assignment of PL lines to particular defects has not been substantiated by modern theory. Using density functional theory (DFT), we investigate from first principles which native defects introduce electronic states within the Cu_2O band gap, and therefore would produce lines in the PL spectrum. We find that the accepted assignments of lines to simple oxygen and copper vacancies are unsupported, and propose a new assignment based on oxygen and copper interstitials, and (one of the possible) split copper vacancies, a significant step towards the use of PL as a diagnostic tool for Cu_2O crystal growth.

1 Introduction

Cu_2O is one of the earliest semiconductors to be studied in detail, with a research history of over 70 years [1, 2]. In that time, it has been of interest for studying fundamental excitonic physics [2], solar cells [3, 4], and most recently Rydberg excitons [5], where it is emerging as a platform for quantum sensing [6], polaritonic devices [7], and microwave-optical conversion [8, 9]. For these quantum applications, microscopic control of the host crystal is crucial, since even small concentrations of defects can alter exciton properties such as lifetimes and coherence [10]. Indeed, sample variability is a central obstacle [10, 11], where the exciton spectra from different samples of Cu_2O differ significantly in the heights of the absorption lines and the number of resolvable lines. This has been shown to be due to charged defects in the crystal [12, 13], com-

monly taken to be copper and oxygen vacancies. The spectra which show the highest- n exciton lines are all seen in natural samples [14, 13]; however samples of such quality are rare. Work continues on the growth of synthetic cuprous oxide [15, 16, 17] to achieve reproducible material quality suitable for scalable quantum devices.

One method for assessing for sample quality is the photoluminescence (PL) spectrum [18, 19, 11]. The PL spectrum in synthetic samples has been measured to contain significant emission of energy less than the band gap, E_g ; emission that is not present in the spectra of high-quality natural samples [11]. This is an indicator of defect states within the band gap due to defects in the crystal structure.

The photoluminescence spectrum of Cu_2O has been studied many times over its history, and 5 main lines have been documented [13, 11, 12, 19, 18, 20, 21, 22, 1], at 1.2 eV, 1.35 eV, 1.5 eV, 1.7 eV, and 1.9 eV, as shown in the sketch in figure 1. It is commonly stated in the field that the line at 1.35 eV is due to the copper vacancy, V_{Cu} , where a single copper atom is missing from the lattice. The lines at 1.5 eV and 1.7 eV are commonly attributed respectively to V_{O}^+ and V_{O}^{2+} , the different charge states of the oxygen vacancy. The assignment of these lines is due to a 1958 study by Bloem [1], which linked changes in line heights to the oxygen pressure during sample growth. In Bloem's samples the heights of the lines at 1.5 eV and 1.7 eV were always in the same ratio, and disappeared in the samples grown in high oxygen pressure. Under the assumption that the only significant native defects were V_{Cu} and V_{O} , he therefore assigned the lines at 1.5 eV and 1.7 eV to V_{O}^+ and V_{O}^{2+} , and the large line at 1.35 eV to the remaining defect, V_{Cu} . However later studies showed that different samples displayed widely varying ratios or even absences of some lines, a discrepancy first noticed by Biccari [23]. For example, the natural sample in Ito et al. [22] showed a bright line for 1.7 eV and no line at all at 1.5 eV, suggesting the two lines were due to different defects. Furthermore Bloem did not speculate on the origin of the line at 1.2 eV, and the line at 1.9 eV has only

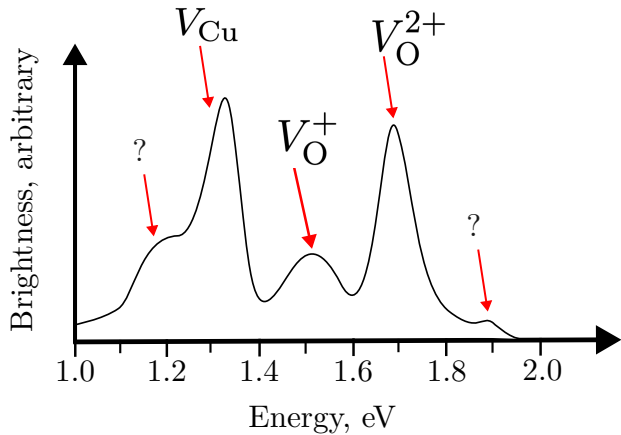


Figure 1: A sketch of an example PL spectrum showing the 4 main lines commonly observed, with the defect assignments made by Bloem [1].

been seen clearly in the recent results of Frazer et al. [19]. Finally, computational studies of Cu_2O [24, 25, 26] using density functional theory (DFT) have shown that a host of native defects can form under various growth conditions, not just V_{Cu} and V_{O} . These discrepancies highlight the need for a re-examination of the origin of these PL lines.

In this work, we pursue the PL line origins from first principles using DFT. We identify which native point defects can, in principle, generate electronic states in the band gap, and therefore which are capable of producing the well known PL lines. Previous DFT studies of defects in Cu_2O identified up to 10 possible native defects [25], and found gap states associated with interstitials as well as vacancies [25, 26]. However, more sophisticated calculations [27] have shown these studies suffered from weak approximations and under-convergence with various DFT parameters, leading to numerical artefacts, something Cu_2O is particularly sensitive to, due to strong electron correlation effects [28, 29]. Moreover, most previous calculations have been performed only in the minimal possible supercell, which overestimates defect concentrations in the material and introduces finite-size effects, and only examine states at the gamma-point of the Brillouin zone, which can lead to mislabelling of gap states.

Building on these earlier studies, we use modern computational resources to: examine all native point defects in $2 \times 2 \times 2$ and $3 \times 3 \times 3$ supercells, to investigate important finite-size effects; examine all defects with HSE-

DFT, a more sophisticated approximation, to correct for band gap underestimation and explore exchange- and correlation-driven effects; analyse the full band structures of each defect, allowing for a more nuanced categorisation of defect states; and study the effect of charge on the band structures of the defect states.

2 Methodology

DFT is the leading theory for calculating the electronic structure of materials and molecules. It is widely used to study the geometry, formation energy, and electronic structure of both point defects and defect complexes in solids [30, 31, 32, 33, 34, 35]. While many experimental measurements are well-reproduced in DFT, such as atomic geometries, some are not usually quantitatively accurate, for example band gaps in semi-conductors. In fact, it is known that transition metal oxides in particular must be treated carefully with DFT [36]. Nevertheless, choices of approximations can be made to mitigate these problems, and when used in a well understood way, can provide significant physical insight into defect-induced states.

When implementing DFT, the key choice to be made is of the treatment of exchange and correlation, via a term called the exchange-correlation (XC) functional. The choices vary in computational cost and accuracy for given observables. In this work, we use both the commonly used generalised gradient approximation of Perdew, Berke and Ernzerhof (PBE) [37], as well as the hybrid functional of Heyd, Scuseria and Ernzerhof (HSE06) [38, 39]. The former is computationally much more efficient, and reproduces well geometries and formation energies. However, PBE significantly underestimates band gaps, which could present an issue in identifying mid-gap defect states. The latter XC-functional, HSE06, is designed to reproduce the band gaps of semiconductors much more accurately, but comes at significantly higher computational cost, so we were only able to employ it for $2 \times 2 \times 2$ supercells. Our approach is to search for defect states that are robust to increases in supercell size, for which we use PBE, and robust to a more complex treatment of exchange and correlation, for which we use HSE.

The plane wave DFT code CASTEP [40] was used to run all the calculations in this work. We used pseudopotentials for the copper and oxygen ions generated using CASTEP's on-the-fly pseudopotentials. Oxygen atoms had a core of helium and copper atoms had a core of argon, and in both cases PBE was used to compute the

atomic core.

Calculations with the Cu_2O unit cell under PBE and ultrasoft pseudopotentials found a relaxed cell size of 4.29 Å, which was the lattice parameter used for all calculations, including those with HSE06. The optimisation of the cell size was considered converged when the change in energy per atom, $dE/d(\text{atom}) < 2 \times 10^{-5}$ eV, and the stress was below 0.1 GPa. For the same calculation, the density of the Monkhorst-Pack (MP) k-point grid and the cutoff energy for the plane wave basis were varied. The total energy was found to be converged to within 1 meV with an MP grid of $7 \times 7 \times 7$ and a plane wave cutoff energy of 1100 eV. Due to the inverse relation between real-space and k-space, the $2 \times 2 \times 2$ and $3 \times 3 \times 3$ supercell calculations needed only MP k-point grids of $4 \times 4 \times 4$ and $2 \times 2 \times 2$ to be similarly converged. The atomic positions for the various defect supercells were also found via geometry optimisation. These optimisations were considered converged when $dE/d(\text{atom}) < 2 \times 10^{-5}$ eV and all forces on atoms were less than 5×10^{-2} eV/Å.

For the HSE06 calculations, due the available computational resources, we used a cutoff of $E_{\text{cut}} = 1000$ eV, as well as a reduced k-point grid sampling of $4 \times 4 \times 4$. This converged the energy difference between the valence band maximum (VBM) and the conduction band minimum (CBM) to within 1 meV, indicating (but unfortunately not guaranteeing) that the band structure has stopped changing in a material way.

The HSE functional contains two parameters that can be adjusted - the Hartree-Fock short-range exchange fraction, α , and screening length ω . We choose to set these at the default values of $\alpha = 0.25$, and $\omega = 0.2 \text{ \AA}^{-1}$ determined from perturbation theory and fits to many materials [39, 41]. Scanlon et al. [26] obtained a more accurate HSE-DFT band gap of $E_g^{\text{HSE}} = 2.12$ eV by changing the fraction of HF exchange from $\alpha = 0.25$ to $\alpha = 0.275$. However, given the systemic problems DFT often has with band gaps, there is no guarantee that a more accurate band gap will lead to better accuracy in any other property of the material. For this reason, we choose to keep the mixing fraction and screening length at their default values.

2.1 Finite size effects

Experimentally, the fractional deviation from stoichiometry in a sample is of the order 10^{-5} [23], which is equivalent to 1 point defect per $\sim 10^4$ unit cells. This level of dilution is not achievable with the resources available for this project. However, for the correct physics, the de-

fects need only be dilute enough to not ‘feel’ the effects of neighbouring defects. To investigate where this dilute limit lies, we model each type of defect under PBE in a $2 \times 2 \times 2$ and $3 \times 3 \times 3$ supercell, and under HSE06 in a $2 \times 2 \times 2$ supercell. As will be seen, the decay on this finite-size effect can be inferred from the difference between the PBE results for the two sizes of supercell with and without the defect, and varies significantly between defects. Unfortunately, since HSE06 is a hybrid functional, it is much more expensive to compute, and so we did not run calculations under HSE06 for $3 \times 3 \times 3$ supercells, since the convergence of the PBE band structure with supercell size can often be used to infer the behaviour of HSE in a larger supercell.

2.2 Spin-orbit coupling

Spin-orbit coupling (SOC) is an important effect in pure Cu_2O , especially for excitons, and is responsible for the various higher energy exciton series above the orange exciton [42] through the splitting of the VBM. However, the numerical difference it makes to band energies is often small, of the order 0.1 eV, and its inclusion introduces significant computational costs, as well as convergence issues associated with a non-collinear spin treatment. These costs made calculations with spin-orbit coupling unfeasible for the $3 \times 3 \times 3$ supercell under PBE and the $2 \times 2 \times 2$ supercell under HSE06, so given its small expected impact on defect state energies, it was not included in the results in this work.

To understand the effect of this choice, SOC calculations were performed for the $2 \times 2 \times 2$ defect supercells under PBE, where it was introduced through CASTEP’s spin-orbit coupling pseudopotentials, with the quantisation axis $(0, 0, 1)$. Examples of the results are compared to those calculations without SOC in figure [FIGURE] of the supplementary material. Across the suite of defects, the inclusion of SOC did not affect the existence or non-existence of a defect state in the band gap; at most, it changed the energy gap of the defect state above the VBM by 0.2 eV. Therefore, we consider there to be a ± 0.2 eV error on the position of the defect states within the band gap due to spin-orbit coupling.

2.3 Charge

Charged point defects are believed to play an important role in modifying the excitonic properties of Cu_2O particularly in the context of recent studies on Rydberg excitons interacting with impurity potentials [12, 13]. We have in-

vestigated how changing the charge state of a defect affects the presence and energy of any in-gap defect levels. Our primary goal here is to determine whether charging qualitatively alters the band structures and the positions of defect levels. We restrict charged-defect calculations to the PBE functional in the $3 \times 3 \times 3$ supercell, where finite-size artefacts are reasonably mitigated and the PBE functional will give us the required qualitative results with the aim to assess trends in the appearance of in-gap states rather than the absolute charge-transition levels. For each defect studied in the $3 \times 3 \times 3$ PBE supercell, we examined charge states in the range $q = -2, \dots, +2$. Structural relaxations were performed for each charged configuration to ensure that any charge-induced local distortions were properly captured. In most cases, particularly for the simple copper and oxygen vacancies, the oxygen anti-site and the second split vacancy, changing the charge state did not introduce new defect levels in the band gap. The band structures differed from their neutral counterparts only by the expected occupation or depletion of already-present states, indicating that none of these defects acquire an in-gap state upon charging. In contrast, some defects that already show in-gap states in the neutral configuration, such as the oxygen interstitials, exhibit systematic shifts in the energies of these states upon charging. For example, the defect levels associated with O interstitials shift rigidly upward by approximately 0.1–0.2 eV per added electron, consistent with the localised nature of the defect orbitals. This behaviour suggests that different charge states of the same defect could give rise to multiple nearby photoluminescence lines in experiment. By comparison, defects whose electronic states are strongly delocalised, such as the copper interstitials, display only small (0.05 eV per electron) charge-induced shifts reflecting their extended real-space character. Overall, the PBE calculations indicate that charging does not generate mid-gap states for defects that lack them in the neutral configuration, but can modify the relative energies of pre-existing localised states. Although the quantitative values of the charged-defect energies are approximate, the qualitative trends identified here form the basis for the charge-dependent defect-level shifts discussed in Sec. 6.

2.4 Formation Enthalpies

To understand which defects are likely to be present in real crystals (and therefore visible in PL) we compute the formation enthalpy, $\Delta H_F(D, q)$, of a defect D with charge q . A low formation enthalpy means the defect can appear in meaningful concentrations under typical growth

conditions, whereas a high formation enthalpy means the defect will be rare, and therefore is unlikely to produce a PL signal even if it produces a defect state in the band gap. In general, it is given by

$$\Delta H_F(D, q) = E(D, q) - E_P + \sum_i n_i (E_i^{\text{elem}} + \Delta \mu_i) + q [\Delta E_F + \epsilon_{\text{VBM}}^P + \Delta v(D)], \quad (1)$$

where $E(D, q)$ is the energy of the supercell with defect D and charge q , E_P is the energy of the neutral perfect supercell of the same size, and n_i is the number of added (negative n_i) or subtracted (positive n_i) atoms of species i . E_i^{elem} is the total energy per atom of each species in its reference state, in this case $\text{O}_2(\text{g})$ and $\text{Cu}(\text{s})$. The additional term $\Delta \mu_i$ changes the chemical potentials depending on the particular chemical potentials of the atoms in the furnace. ΔE_F represents a hypothetical change in the Fermi level, for example from an applied voltage. To calculate the cost of charging the defect, we add ϵ_{VBM}^P , the eigenenergy of the VBM in the pure supercell at Γ , which represents the chemical potential at which electrons are added to or subtracted from the bulk crystal. Finally, the term $\Delta v(D)$ ensures the potentials for the defect supercells are each aligned with the bulk cell. It is defined here as the difference between two low-lying oxygen 2s energy levels in the perfect and defect supercells, $\Delta v(D) = \tilde{\epsilon}_{2s}^P - \tilde{\epsilon}_{2s}^{\text{far}}(D)$, where $\tilde{\epsilon}$ represents averaging the energy over the Brillouin zone. The 2s level used for the defect supercell is on an oxygen atom far from the defect, to ensure it is most comparable to the energy level in the bulk.

The chemical potentials, $\Delta \mu_i$, which represent the growth environment, are subject to several inequalities to prevent precipitates forming in the furnace. To avoid precipitation of O_2 and Cu metal,

$$\Delta \mu_{\text{Cu}} \leq 0, \text{ and} \quad (2)$$

$$\Delta \mu_{\text{O}} \leq 0. \quad (3)$$

Likewise, to avoid precipitation of CuO , it must be kept such that

$$\Delta \mu_{\text{Cu}} + \Delta \mu_{\text{O}} \leq \Delta H_F(\text{CuO}). \quad (4)$$

Finally, in equilibrium when forming Cu_2O it must be true that

$$2\Delta \mu_{\text{Cu}} + \Delta \mu_{\text{O}} = \Delta H_F(\text{Cu}_2\text{O}). \quad (5)$$

Along the line defined by equation 5, the endpoints correspond to the physically important extremes (Cu rich/O

poor and Cu poor/O rich) which bracket realistic growth conditions.

	Cu rich/O poor	Cu poor/O rich
$\Delta\mu_{\text{Cu}}$, eV	0	-0.33
$\Delta\mu_{\text{O}}$, eV	-1.80	-1.30

The elemental chemical potentials $\mu_{\text{Cu}}^{\text{elem}}$ and $\mu_{\text{O}}^{\text{elem}}$ are obtained from the energy per atom of the ‘natural’ state of the elements, in this case O_2 and metallic Cu. For consistency, their geometries were first optimised under PBE, giving a lattice constant of 3.63 Å for Cu and a bond length of 1.21 nm for O_2 , resulting in $E_{\text{Cu}}^{\text{elem}} = 1680.93$ eV/atom and $E_{\text{O}}^{\text{elem}} = 436.80$ eV/atom.

2.5 Criteria for a defect state

Identifying a genuine defect-induced electronic state within the Cu_2O band gap requires care, given the well-known artefacts that arise in supercell calculations. Supercells inevitably introduce folded host bands and additional states unrelated to the defect, while finite-size interactions can shift or distort the energies of the true defect levels. To avoid misinterpretation, we adopt a criterion: a state is classified as a genuine defect level only if it consistently appears between the bulk valence-band maximum (VBM) and the bulk conduction-band minimum (CBM) across both combinations of exchange–correlation functional (PBE and HSE06) and supercell size, and if its presence cannot be attributed to band folding or to perturbations arising from artificially high defect concentrations. This approach ensures that only those states that persist under both changes in the computational method and dilution of the defect are retained as physically meaningful.

To apply this criterion reliably, each defect supercell band structure is compared directly with the corresponding pure supercell band structure. This comparison allows us to distinguish genuinely new states induced by the defect from bands that arise simply due to the modified Brillouin zone or the additional electrons in the supercell. States that remain nearly dispersion-less across the Brillouin zone, shift little with increasing supercell size, and remain separated from folded bulk states provide strong evidence of real-space localisation and are therefore likely to survive in the dilute-defect limit. Conversely, states that are strongly dispersive, appear only in smaller supercells, or shift appreciably when changing the XC functional or supercell size are treated as artefacts of finite-size effects or band folding and are not classified as true

defect states. Applying this methodology, only the oxygen interstitials satisfy the full set of criteria, producing well-defined in-gap states for all tested functionals and supercell sizes. Other defects occasionally produce states that appear promising at a single level of theory but fail the consistency test; these are designated as ambiguous cases and are discussed separately.

3 DFT on pure Cu_2O

Before analysing defects we establish the DFT descriptions of bulk Cu_2O itself. This serves two purposes: first, it provides reference band structures to compare with defect supercells; and second, it allows us to determine which of the features of the pure band structure are robust with respect to supercell enlargement. This will become crucial when identifying spurious states.

In figure 2 we calculate the band structures of the pure crystal for the $2 \times 2 \times 2$ and $3 \times 3 \times 3$ supercells under PBE, and the $2 \times 2 \times 2$ supercell under HSE06, since these are the configurations for which we calculate the defect supercell band structures, without spin-orbit coupling. Band structures are a way of mapping the energy-momentum space of the electrons, and are constructed by plotting the energy eigenvalues along a path around the Brillouin zone. The path taken in this work is between the high symmetry points $X = (1, 0, 0)\pi/a$, $R = (1, 1, 1)\pi/a$, $M = (1, 1, 0)\pi/a$, and $\Gamma = (0, 0, 0)$, where a is the lattice parameter of the respective supercell. The focus here is, in particular, on the gamma point, since that is where the gap in Cu_2O is located.

The band gap calculated under PBE is $E_g^{\text{PBE}} = 0.50$ eV (which we will call the PBE gap), significantly less than the experimental gap of 2.18 eV, but in good agreement with other PBE studies of Cu_2O [24, 25]. Inaccurate band gaps are a problem inherent in Kohn-Sham DFT, but such a significant underestimation is an indication that Cu_2O is a strongly-correlated material, hence why it is important to include hybrid functionals like HSE06 in our analysis. Despite this, PBE-DFT is known to reproduce well the shapes and orderings of bands, and so these are the things we are trying to extract from our simulations. Furthermore, the existence of mid gap defect levels is often determined by relative ordering, not always by absolute gap.

The band gap calculated under HSE is $E_g^{\text{HSE}} = 1.60$ eV (which we will call the HSE gap), which is more comparable to the experimental gap than the PBE gap is, but unsurprisingly not exact. This result is also less than

the HSE gap found by Scanlon [26] (2.12 eV), but the discrepancy is accounted for by the different HSE parameters used in that study. Analysis of the density of states reveals that the top of the valence band is predominantly of copper 3d and oxygen 2p character, and the bottom of the conduction band is of copper 4s and copper 3d character. The interplay between the 4s and 3d orbitals is characteristic of strongly correlated materials, and in which orbitals the electrons lie in the ground state is sensitive to our treatment of correlation effects, highlighting the importance of employing hybrid functionals.

It is important to note that the boundaries of the (first) Brillouin zone are at $\pm\pi/a$, so for larger supercells, the Brillouin zone is smaller. This has two effects on the band structure of larger supercells: first, bands appear flatter, because the x-axis covers less reciprocal-space distance. Second, since the bands ‘reflect’ off the Brillouin zone boundaries, the reduced boundaries cause additional bands to appear in the band structure (known as band folding). Furthermore, the additional electrons present in the larger supercell adds additional bands as well. All 3 effects can be seen by comparing the $2 \times 2 \times 2$ and $3 \times 3 \times 3$ supercell PBE band structures in figure 2. For these reasons, it is imperative that we compare each defect supercell with the corresponding bulk supercell, in order to discern which effects are a result purely of the defect.

4 The Defects

In this section we present the defect-induced changes to the electronic structure, identifying which of the point defects introduce gap states and which do not. These are all the native single-point defects, plus the split vacancies: the copper and oxygen vacancies, V_{Cu} and V_{O} , where a single atom is missing from the lattice; the anti-sites, Cu_O (O_{Cu}) where a copper (oxygen) atom is in the usual place of an oxygen (copper) atom; the interstitial atoms, Cu_i^{oct} , Cu_i^{tet} , O_i^{oct} and O_i^{tet} , where a copper or oxygen atom is inserted into the stoichiometric lattice in one of two different sites, labelled tetrahedral and octahedral after the way they coordinate with neighbouring copper atoms; and the split copper vacancies, $V_{\text{Cu}}^{s,1}$ and $V_{\text{Cu}}^{s,2}$, defect complexes formed from two adjacent copper vacancies with a copper interstitial at their midpoint. $V_{\text{Cu}}^{s,1}$ is formed when the copper vacancies are formed around different oxygen atoms, and $V_{\text{Cu}}^{s,2}$ is formed when the copper vacancies are formed around the same oxygen atom. Only the former case is studied in the literature [26, 25, 27, 43].

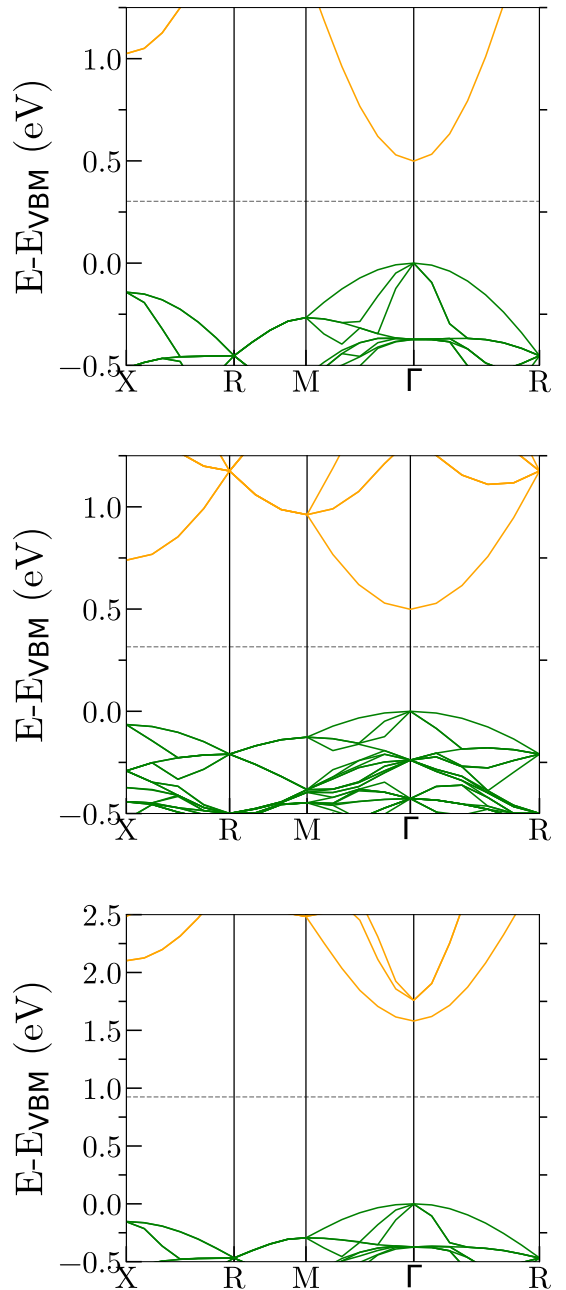


Figure 2: Band structures for pure Cu_2O in supercells. From top to bottom: PBE band structure in a $2 \times 2 \times 2$ supercell; PBE band structure in a $3 \times 3 \times 3$ supercell; HSE06 band structure in a $2 \times 2 \times 2$ supercell. Occupied states are shown in green and unoccupied states are shown in orange. The dotted line denotes the Fermi level.

Based on the criteria we set out in section 2.5, we sort the results from each defect into 3 categories: no gap states, gap states, and inconclusive results. The defects in the first category meet none of the criteria, in that they generate no state between the VBM and the CBM at either supercell size under PBE, nor under HSE. The defects in the second category meet all our criteria. They generate low dispersion, well localised gap states at all levels of theory. The third category is for defects that do not meet all of the criteria, such as exhibiting gap states only under the HSE XC-functional, or gap states who's dispersion is too high to infer the behaviour in the dilute limit. The details of each defect is discussed within each category.

4.1 No defect states in the band gap

	V_{Cu}	V_O	$V_{Cu}^{s;2}$	O_{Cu}
ΔH_F , eV (Cu rich)	0.39	0.66	1.47	3.75
ΔH_F , eV (Cu poor)	0.05	1.16	1.25	2.92
Charge	-1	0	-1	-1
PBE, $2 \times 2 \times 2$	No	No	No	No
PBE, $3 \times 3 \times 3$	No	No	No	No
HSE06, $2 \times 2 \times 2$	No	No	No	No

Table 1: For the negative defect results: the formation energy of the lowest energy charge state, the charge of that state, and with whether or not the given level of theory predicts defect states in the band gap.

4.1.1 Copper vacancy

The band structures for the simple copper vacancy for $2 \times 2 \times 2$ and $3 \times 3 \times 3$ supercells under PBE and for the $2 \times 2 \times 2$ supercell under HSE06 are seen in figure 3. The occupied states are shown in green and the unoccupied states are shown in orange. In contradiction with the commonly held PL line assignments, across all three band structures, we see V_{Cu} does not introduce a clear electronic state in the band gap. In the smaller supercell under both PBE and HSE06 we see that V_{Cu} perturbs the valence band such that the VBM becomes slightly peaked. Were we only to look at the eigenvalues at the Γ point, it would be easy to believe that a defect state has appeared in the band gap just above the valence band. However, when we dilute the defect further in the $3 \times 3 \times 3$ supercell under PBE, we see the structure return to be identical to the valence and conduction bands in the bulk crystal (fig. 2), demonstrating that the peaking of the valence band is merely a finite-size effect caused by an unphysical effective

density of defects. Given the similarity between the PBE and HSE upper valence bands in the $2 \times 2 \times 2$ supercell, we can be confident that HSE is not introducing new physics which is absent from the PBE level of analysis, and that the peak in the valence band under HSE is also a finite-size effect.

Across all three band structures we also see that the top of the valence band is partially unoccupied. This is expected, since the removal of a copper atom leaves an odd number of electrons. Under PBE the VBM is spin degenerate and half occupied, but under HSE the top state is actually only of one spin channel, a consequence of the spin splitting caused by Hartree-Fock exchange near the Fermi level. Neither effect would produce photoluminescence lines of energy less than E_g , but, as has been reported many times before [26, 24, 44], they are responsible for much of the p-type conductivity observed in the semiconductor literature on cuprous oxide [45].

For the PBE $3 \times 3 \times 3$ supercell, charges of up to ± 2 electrons had no effect on the band structure of V_{Cu} , other than to occupy or un-occupy the bands seen in the neutral band structures. Therefore, there is no reason to believe charged V_{Cu} would produce any PL lines either. These results provide strong evidence that V_{Cu} does not produce any mid-gap states under any realistic charge state, supercell size, or XC-functional, and therefore cannot be the origin of the PL peak at 1.35 eV.

4.1.2 Oxygen vacancy

As seen in figure 4, the oxygen vacancy produces no gap state across all 3 levels of analysis. In the $2 \times 2 \times 2$ supercells, the effect of the oxygen vacancy when compared to the bulk band structures is to flatten the CBM and open the gap, to 0.78 eV (PBE) and 1.83 eV (HSE), greater than the PBE gap and HSE gap respectively. However, the PBE $3 \times 3 \times 3$ supercell band structure returns almost exactly to the bulk behaviour, with a gap of 0.56 eV, demonstrating that the effects seen in the smaller supercells are finite-size effects, not genuine defect states. While it is hard to be certain how dilute the defect would need to be for the gap to return to its bulk value, we can be certain that larger supercells will not introduce states inside the band gap if they are not seen in these artificially high defect concentrations.

For the PBE $3 \times 3 \times 3$ supercell, charges of up to ± 2 electrons had no effect on the band structure of V_O , other than to occupy or un-occupy the bands seen in the neutral band structures. Since no defect state appears in the neutral defect supercell, there is no defect state associated

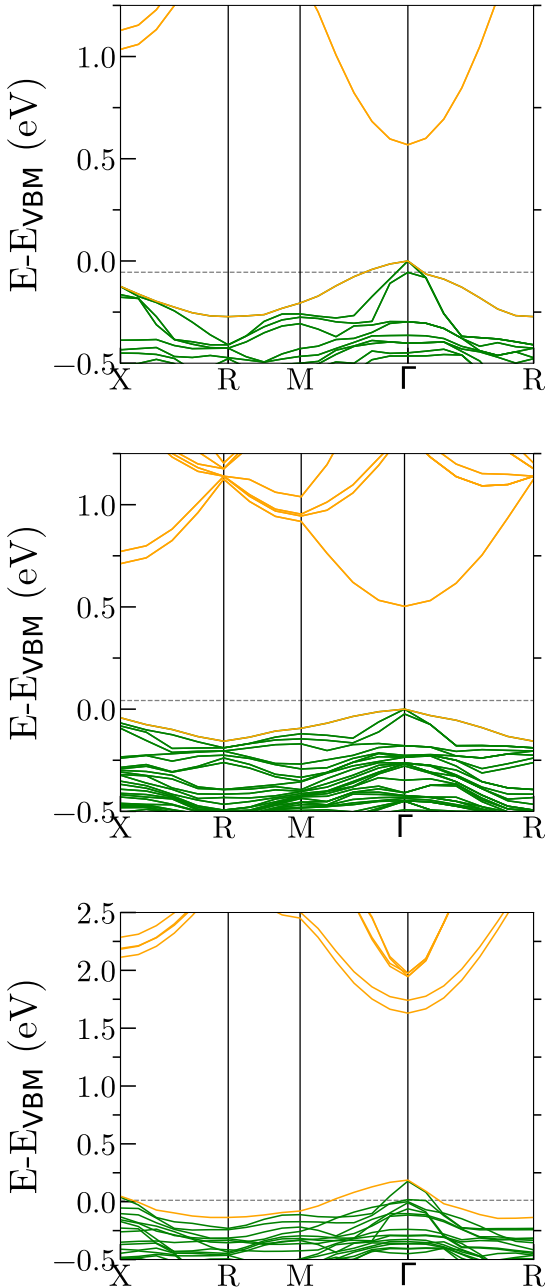


Figure 3: Band structures for the simple copper vacancy, V_{Cu} . From top to bottom: PBE band structure in a $2 \times 2 \times 2$ supercell; PBE band structure in a $3 \times 3 \times 3$ supercell; HSE06 band structure in a $2 \times 2 \times 2$ supercell. Occupied bulk states are shown in green and unoccupied bulk states are shown in orange. The dotted line denotes the Fermi level. The simple copper vacancy does not exhibit defect states in the band gap.

with the charge oxygen vacancy either. Therefore, there is no reason to believe charged V_O , including V_O^+ and V_O^{2+} , would produce any PL lines either.

4.1.3 Other

The second form of the split copper vacancy, $V_{\text{Cu}}^{s,2}$, as well as the oxygen anti-site, O_{Cu} , produce no defect states in the band gap across all 3 levels of analysis. In fact they both behave very similarly to V_{Cu} , including the peaking of the VBM in small supercells and introducing holes into the valence band. Charges of $\pm 2e$ also had no material effect on their band structures. The band structures for these defects can be seen in the supplementary material.

4.2 Defect states in the band gap

	O_i^{tet}	O_i^{oct}
ΔH_F , eV (Cu rich)	1.56	2.00
ΔH_F , eV (Cu poor)	1.06	1.50
Charge	+1	0
PBE, $2 \times 2 \times 2$	Yes	Yes
PBE, $3 \times 3 \times 3$	Yes	Yes
HSE06, $2 \times 2 \times 2$	Yes	Yes

Table 2: For the positive defect results: the formation energy of the lowest energy charge state, the charge of that state, and with whether or not the given level of theory predicts defect states in the band gap.

4.2.1 Oxygen interstitials

Both geometries for these interstitials show clear defect states in the band gap across both supercell sizes and for both PBE and HSE xc-functionals. The band structures for the two geometries of the oxygen interstitials are shown in figures 5 and 6. The occupied bulk states are shown in green and the unoccupied bulk states are shown in orange. The occupied defect states are shown in blue and the unoccupied defect states are shown in red. Both geometries produce 3 well localised spin-degenerate states in the gap, 2 occupied and 1 unoccupied, which are easily understood as the 2P electrons of the additional oxygen atom.

As can be seen for O_i^{oct} (fig. 5), the unoccupied defect state remains deep in the band gap for the $3 \times 3 \times 3$ supercell. Along with the fact that it is so flat, meaning it is very well localised, we can be confident it is not a consequence of neighbouring defects interacting with each other but a genuine, additional, local electronic state that

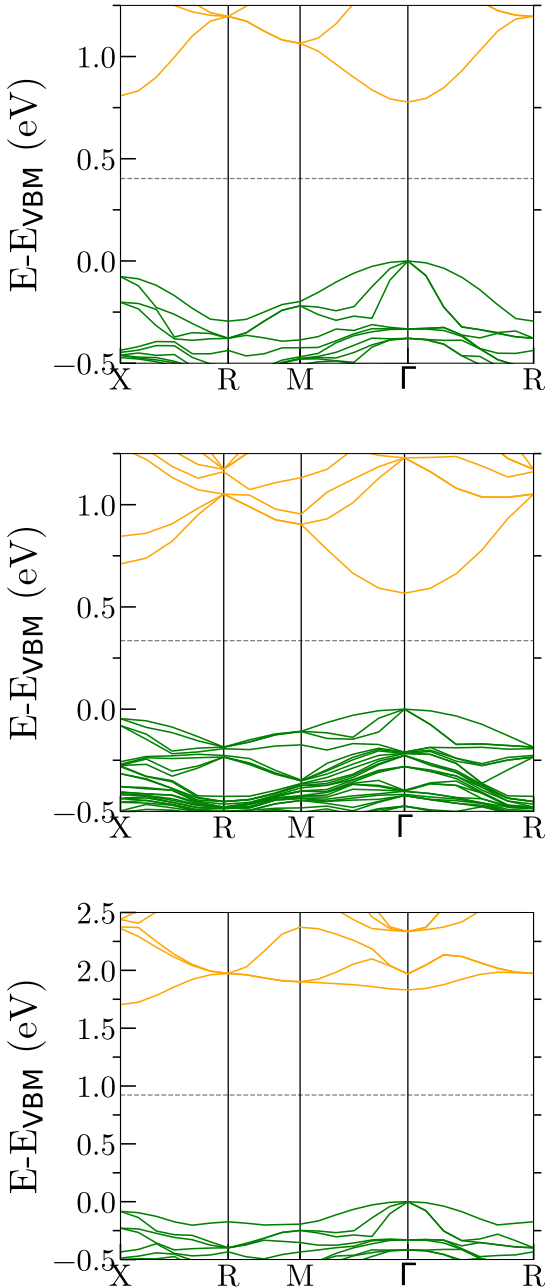


Figure 4: Band structures for the oxygen vacancy, V_O . From top to bottom: PBE band structure in a $2 \times 2 \times 2$ supercell; PBE band structure in a $3 \times 3 \times 3$ supercell; HSE06 band structure in a $2 \times 2 \times 2$ supercell. Occupied bulk states are shown in green and unoccupied bulk states are shown in orange. The dotted line denotes the Fermi level. The oxygen vacancy does not exhibit defect states in the band gap.

would exist in the dilute defect limit. The two occupied defect states for O_i^{oct} are degenerate with the VBM at Γ . Across all three calculations the defect had no effect on the band gap, lending further evidence that the states would not move in relation to the band gap in the dilute limit.

In contrast, figure 6 shows that all three defect states introduced by O_i^{tet} exist firmly inside the appropriate bulk gap and could even produce several distinct photoluminescence lines in experiments. All three states localise further from the $2 \times 2 \times 2$ supercell to the $3 \times 3 \times 3$ supercell under PBE, and their similarity under HSE suggests they would do the same. The gaps in the $2 \times 2 \times 2$ supercells are slightly larger than their bulk values, but in the $3 \times 3 \times 3$ supercell the band gap returns to the bulk PBE value, so we assume the same for HSE.

For the oxygen interstitials in the $3 \times 3 \times 3$ PBE supercell, we found all 3 defect levels shifted rigidly up for each additional electron and down for each removed electron, up to ± 2 electrons, indicating that the different charge states of these defects could show distinct lines in the PL spectrum. The shift was ~ 0.2 eV for O_i^{tet} and ~ 0.1 eV for O_i^{oct} per electron. The exception to this rule was $(O_i^{oct})^+$, which maintained the same energy of in-gap defect state as O_i^{oct} .

4.3 Inconclusive results

	Cu_i^{tet}	Cu_i^{oct}	$V_{Cu}^{s:1}$	Cu_O
ΔH_F , eV (Cu rich)	2.17	1.35	0.69	3.80
ΔH_F , eV (Cu poor)	2.50	1.69	0.35	4.63
Charge	+1	+1	-1	+1
PBE, $2 \times 2 \times 2$	Yes	Yes	No	No
PBE, $3 \times 3 \times 3$	Inc.	Inc.	No	No
HSE06, $2 \times 2 \times 2$	Yes	Yes	Yes	Inc.

Table 3: For the inconclusive defect state results: the formation energy of the lowest energy charge state, the charge of that state, and with whether or not the given level of theory predicts defect states in the band gap. “Inc.” is short for inconclusive.

4.3.1 Copper interstitials

The copper interstitials, both in the octahedral (figure 7) and tetrahedral (figure 8) arrangements, produce similar distortions from the bulk structure, so we will discuss them together.

Under PBE, for the $2 \times 2 \times 2$ supercell, a half-occupied state appears at 0.32 eV above the VBM for the octahe-

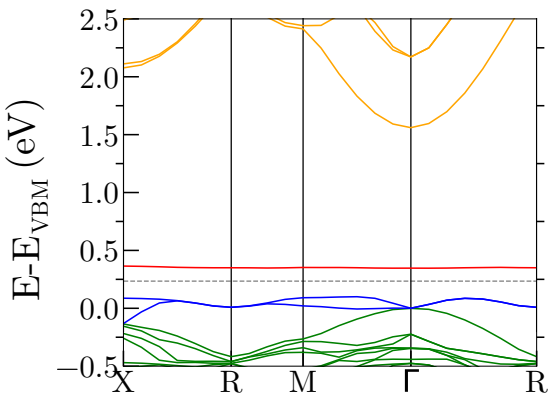
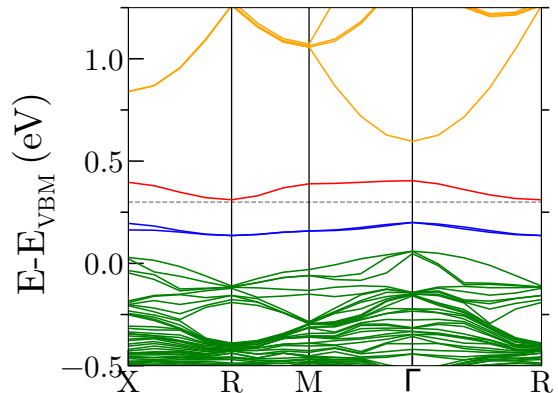
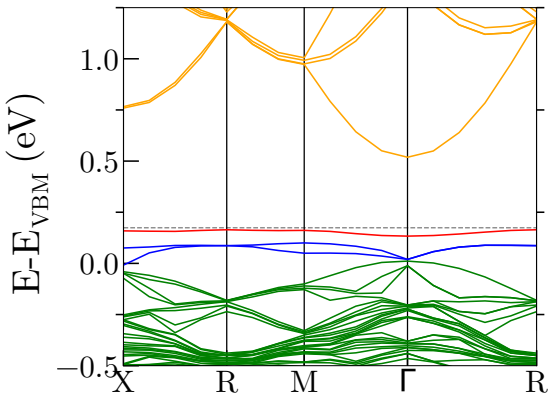
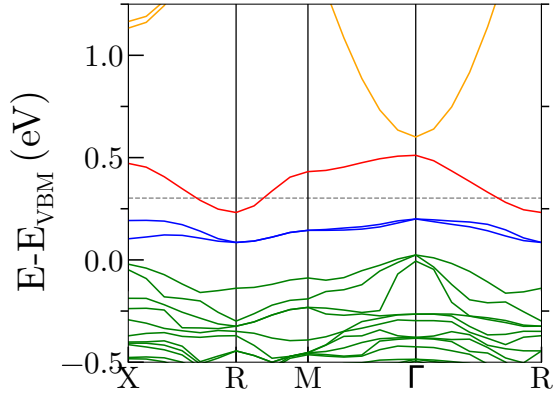
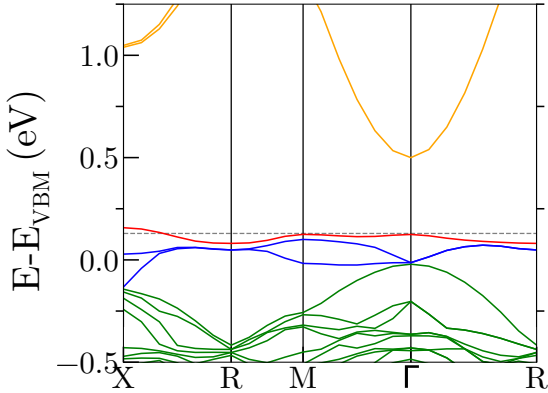


Figure 5: Band structures for the octahedral form of the oxygen interstitial, O_i^{oct} . From top to bottom: PBE band structure in a $2 \times 2 \times 2$ supercell; PBE band structure in a $3 \times 3 \times 3$ supercell; HSE06 band structure in a $2 \times 2 \times 2$ supercell. Occupied bulk states are shown in green, unoccupied bulk states in orange, occupied defect states in blue and unoccupied defect states in red.

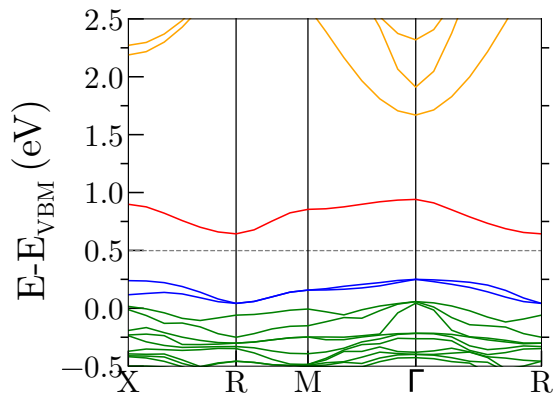


Figure 6: Band structures for the tetrahedral form of the oxygen interstitial, O_i^{tet} . From top to bottom: PBE band structure in a $2 \times 2 \times 2$ supercell; PBE band structure in a $3 \times 3 \times 3$ supercell; HSE06 band structure in a $2 \times 2 \times 2$ supercell. Occupied bulk states are shown in green, unoccupied bulk states in orange, occupied defect states in blue and unoccupied defect states in red.

dral arrangement and 0.34 eV for the tetrahedral arrangement, well within the bulk PBE gap at Γ . The state has a very wide dispersion, indicating a large extent in real space, and so a large finite-size effect. Comparing these band structures to the bulk crystal, we also see that the CBM is missing, so we could think that these defect states are simply a perturbation of the CBM that would return to bulk behaviour in the dilute limit.

Interestingly, the defect states are somewhat robust to increasing the supercell size, indicating that this state could exist even in the dilute defect limit. The band increases to 0.42 eV for octahedral and 0.40 eV for tetrahedral for the $3 \times 3 \times 3$ PBE supercell, still less than but closer to the bulk PBE gap. Comparing again to the bulk $3 \times 3 \times 3$ PBE supercell band structure, a band appears at the bottom of the conduction band which could be the bulk CBM returning to its bulk behaviour. One can imagine two scenarios for the dilute limit under PBE: the defect state rejoins the conduction band as the bulk CBM; or the state remains within the PBE gap and the bulk CBM emerges from the conduction band. A further study of the $4 \times 4 \times 4$ supercell would be needed to distinguish between these two.

The HSE analysis gives us a different angle to understand these defects. The half-occupied state predicted by PBE is split by Hartree-Fock exchange into a lower occupied spin state and an upper unoccupied spin state. The occupied spin states are 0.93 eV and 0.98 eV above the VBM for Cu_i^{oct} and Cu_i^{tet} respectively, and the unoccupied ones not only resemble the bulk CBM but are exactly the bulk HSE gap above the VBM.

For both copper interstitials, in the PBE $3 \times 3 \times 3$ supercell, charging the defect by adding (subtracting) up to 2 electrons raised (lowered) the energy of the defect state by 0.05 eV per electron. This introduces the possibility that different charge states of the copper interstitials could produce a cluster of neighbouring PL lines. However, the behaviour of the charged defects may be significantly different under HSE, given the large spin splitting of the defect level.

The strong dispersion of these states indicates that the electron wavefunctions are delocalised across the supercell, interacting at long range with periodic copies of the defect site. These finite-size effects violate our criterion for a genuine defect state, as we cannot be sure of the behaviour in the dilute limit. Our cautious interpretation of such results is that the interstitial copper atoms provide an additional, local binding of one of the CBM states, leading to a local state in the band gap, near in energy to the CBM, which extends over several unit cells in real

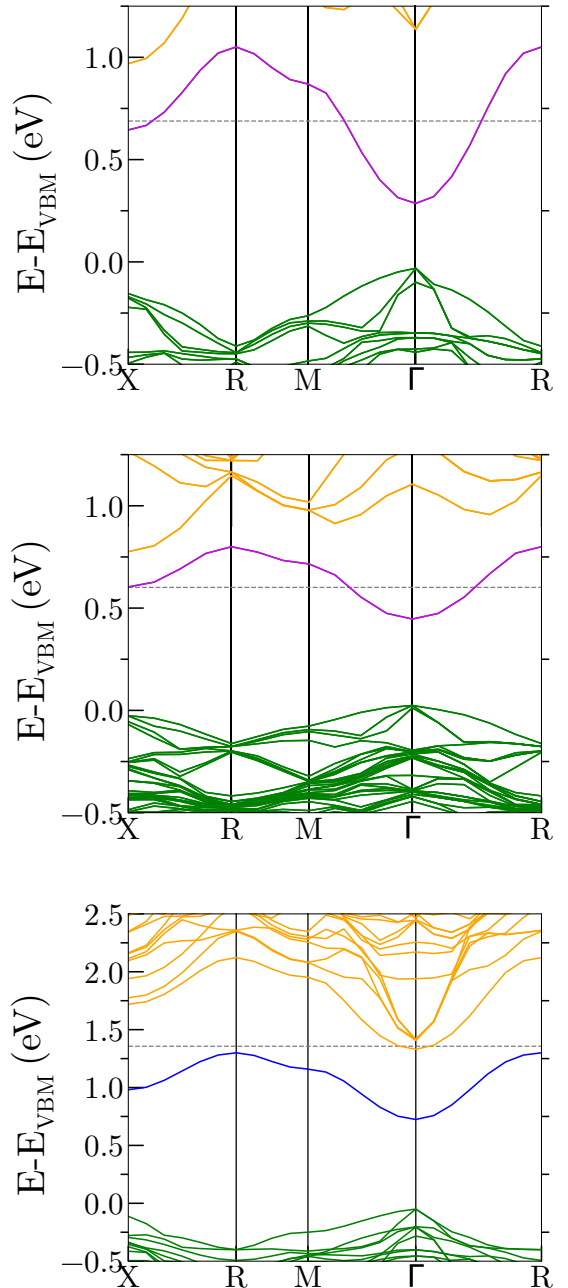


Figure 7: Band structures for the octahedral form of the copper interstitial, Cu_i^{oct} . From top to bottom: PBE band structure in a $2 \times 2 \times 2$ supercell; PBE band structure in a $3 \times 3 \times 3$ supercell; HSE06 band structure in a $2 \times 2 \times 2$ supercell. Occupied bulk states are shown in green, unoccupied bulk states in orange, occupied defect states in blue and half-occupied defect states in purple.

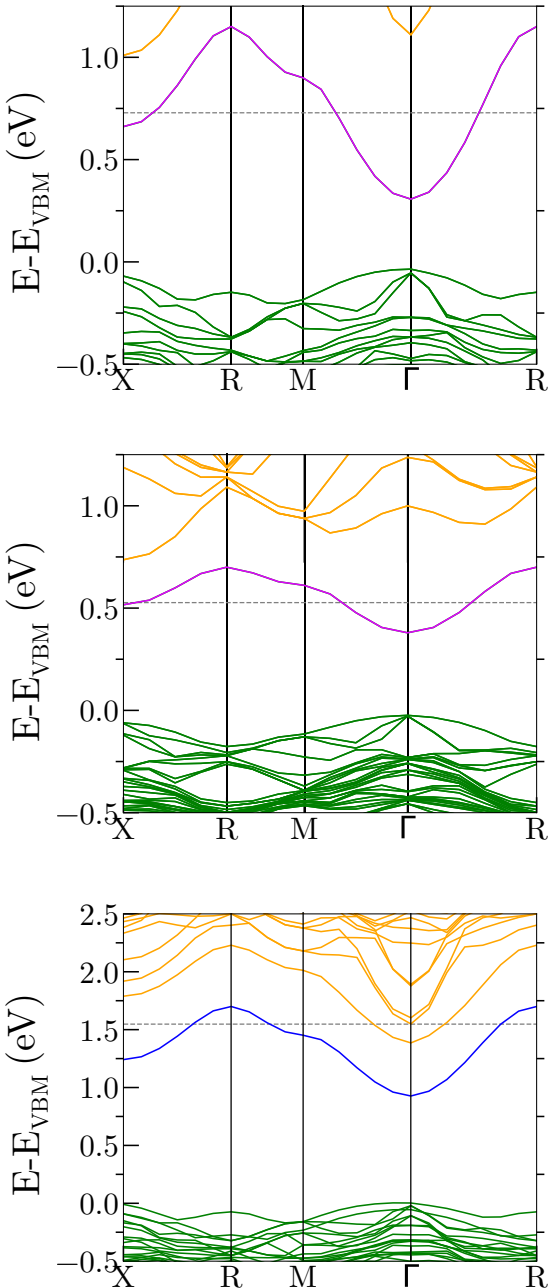


Figure 8: Band structures for the tetrahedral form of the copper interstitial, Cu_i^{tet} . From top to bottom: PBE band structure in a $2 \times 2 \times 2$ supercell; PBE band structure in a $3 \times 3 \times 3$ supercell; HSE06 band structure in a $2 \times 2 \times 2$ supercell. Occupied bulk states are shown in green, unoccupied bulk states in orange, occupied defect states in blue and half-occupied defect states in purple.

space. However, larger supercell calculations would be required to verify this analysis.

4.3.2 First split copper vacancy

Under PBE, the band structure for the first split copper vacancy (where the copper atoms were bonded to different oxygen atoms), seen in figure 9, looks very similar to the simple copper vacancy and the second split copper vacancy. The only difference is that the VBM for $V_{\text{Cu}}^{s;1}$ is raised at R to the same energy as at Γ in the $2 \times 2 \times 2$ supercell. The VBM mostly restored to that of the bulk in the $3 \times 3 \times 3$, but even if this persists in the dilute limit it will not have an effect on the photoluminescence. Like the other copper vacancies, the VBM also becomes partially unoccupied, contributing to native p-type conductivity, but not to photoluminescence.

Under HSE, a defect state appears in the HSE gap 0.35 eV above the valence band maximum. The band is very flat and well localised, and only exists for one of the spin channels. This is in excellent agreement with Isseroff and Carter [27], who found a defect state with only one allowed spin with a line in the density of states 0.57 eV above the VBM. The fact that this state only exists for one spin channel suggests a similar concern as for the copper interstitials. Hybrid functionals like HSE struggle to accurately treat partially-occupied states, since they encounter divergences in the derivative of the energy at the Fermi level, so this defect state could be an artefact. However, the other two copper vacancies have a partially-occupied VBM and do not exhibit such an artefact under HSE, which encourages us to believe the defect state for $V_{\text{Cu}}^{s;1}$ is physical and due to some physics captured by HSE not present under PBE.

Under PBE in the $3 \times 3 \times 3$ supercell, charges of up to ± 2 electrons had no effect on the band structure, other than to occupy or un-occupy the states present in the neutral band structure. Due to restrictions in computational resources, we did not investigate charge states under HSE, which for $V_{\text{Cu}}^{s;1}$ could be important. Since HSE can have problems treating states which cross the Fermi level, it is possible that the unoccupied defect level present under HSE in the neutral defect could return to the valence band when occupied.

4.3.3 Copper replacing oxygen

The copper anti-site Cu_O introduces a myriad of defect states in the gap, as seen in figure [FIGURE] of the supplementary material. However, under PBE, it also greatly

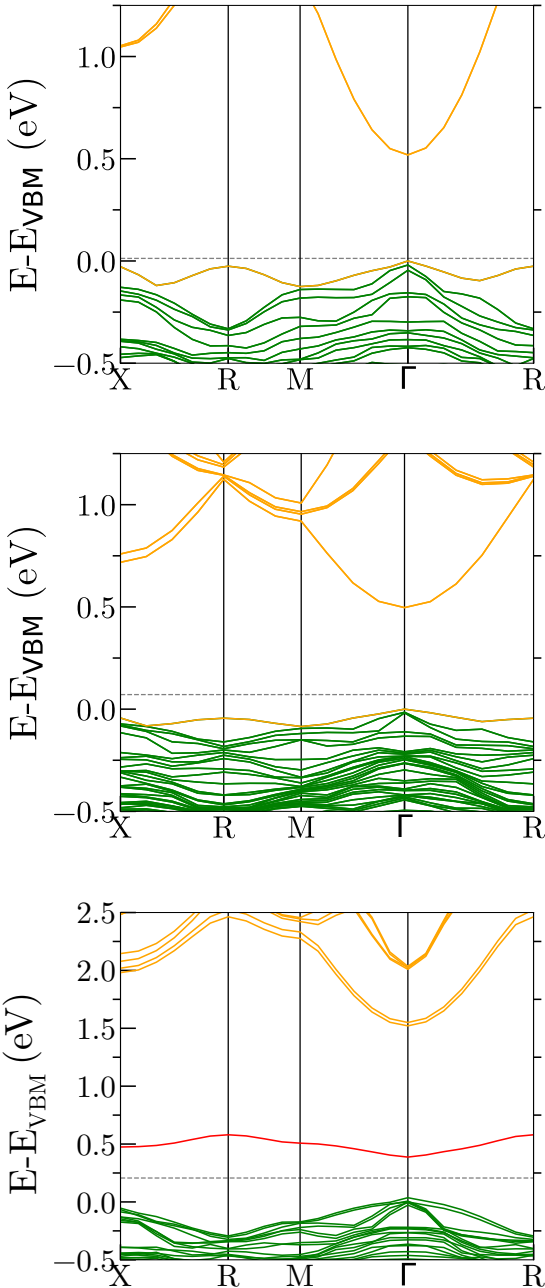


Figure 9: Band structures for the first form of the split copper vacancy, $V_{\text{Cu}}^{s,1}$. From top to bottom: PBE band structure in a $2 \times 2 \times 2$ supercell; PBE band structure in a $3 \times 3 \times 3$ supercell; HSE band structure in a $2 \times 2 \times 2$ supercell. Occupied bulk states are shown in green, unoccupied bulk states are shown in orange, and unoccupied defect states are shown in red. The dotted line denotes the Fermi level.

increases the gap to above the bulk PBE gap, so we do not consider them potentially responsible for any PL lines. Under HSE, there are many possible emitting states, but they display much of the same character as the states in the $2 \times 2 \times 2$ supercell under PBE, which changed dramatically when increasing to the $3 \times 3 \times 3$ supercell. Therefore, we do not assign any weight to the states seen under HSE. The effect of charge in the $3 \times 3 \times 3$ PBE supercell on Cu_O is slightly complicated. Broadly, positive charge leaves no possible photoluminescent states, but negative charge does create a possible high-energy photoluminescent state. However, with formation energies of 4-5 eV, these states are very unlikely to manifest in the crystal.

5 Discussion

There are 4 PL lines commonly observed across authors and samples [1, 22, 18, 19, 20, 21] at ~ 1.2 eV, ~ 1.35 eV, ~ 1.5 eV, and ~ 1.7 eV, and a fifth small line observed by Frazer et al [19] at ~ 1.9 eV. No one has yet identified clear trends in line sizes against growth conditions. Natural samples seem to be more often dominant in 1.7 eV emission [19, 22], Li et al. [21] and Koirala et al. [20] synthesise samples that are dominant in 1.7 eV emission, and Frazer et al. [19], Ito et al. [46] and Bloem [1, 23] synthesise samples with all kinds of emissions. The emissions at 1.35 eV and the emission at 1.7 eV are usually stronger than the other 3, and the line at 1.35 eV is rarely seen without the shoulder at 1.2 eV. The only potential trend was documented by Bloem [1], who found that the line at 1.7 eV disappeared in samples grown above a threshold oxygen pressure. However, with only 6 crystal samples, it is not a strong conclusion, and no other study investigates the relationship between PL and chemical growth conditions.

Conventionally, the line at 1.35 eV is assigned to the simple copper vacancy, V_{Cu} , and the lines at 1.5 eV and 1.7 eV are assigned to the oxygen vacancy, V_{O} . These assignments are due to Bloem [1], and are based on 3 arguments: the only two meaningful native defects in Cu_2O are the simple copper and oxygen vacancies; Bloem observed the line heights at 1.5 eV and 1.7 eV to always be in the same ratio; and the peak at 1.7 eV disappeared at high oxygen pressure. The first two of these arguments are now known not to be true. As can be seen in table 4 (and other studies [26, 25]), many native defects can form in Cu_2O with formation enthalpies comparable to the vacancies, and therefore possibly contribute to PL. Furthermore, every other study of PL in Cu_2O [46, 18, 19, 20, 21]

	V_{Cu}	$V_{\text{Cu}}^{s;1}$	$V_{\text{Cu}}^{s;2}$	V_{O}	Cu_i^{tet}	Cu_i^{oct}	O_i^{tet}	O_i^{oct}	Cu_{O}	O_{Cu}
$\Delta H_F^{(q)}$, eV (O poor)	0.39	0.69	1.47	0.66	2.17	1.35	1.56	2.00	3.80	3.75
$\Delta H_F^{(q)}$, eV (O rich)	0.05	0.35	1.14	1.16	2.50	1.69	1.06	1.50	4.63	2.92
Charge	-1	-1	-1	0	+1	+1	+1	0	+1	-1
PBE $2 \times 2 \times 2$	No	No	No	No	Yes	Yes	Yes	Yes	No	No
PBE $3 \times 3 \times 3$	No	No	No	No	Inc.	Inc.	Yes	Yes	No	No
HSE06 $2 \times 2 \times 2$	No	Yes	No	No	Yes	Yes	Yes	Yes	Inc.	No

Table 4: For each defect: the enthalpy of formation of the lowest enthalpy charge state at the two extremes of growth conditions; the charge of the lowest enthalpy charge state; whether or not the given level of theory predicts a defect state in the band gap. The abbreviation “Inc.” is short for inconclusive.

has found the lines at 1.5 eV and 1.7 eV in a variety of different ratios. Therefore, the evidence for the assignment of V_{Cu} and V_{O} to these peaks is weak.

In direct contradiction with the conventional assignments, there is no evidence within our state-of-the-art DFT calculations that the oxygen vacancy V_{O} , simple copper vacancy V_{Cu} , second split copper vacancy $V_{\text{Cu}}^{s;2}$, or oxygen anti-site O_{Cu} give rise to any states within the bulk band gap (table 4) nor would produce any signal in photoluminescence experiments. Therefore, there appears to be no reason to label the photoluminescence lines observed in experiments with either V_{Cu} or with V_{O} . In fact, given their small perturbations in $2 \times 2 \times 2$ supercells for both XC-functionals and lack of effect on the band structure of the $3 \times 3 \times 3$ supercell, it is unlikely they would have any effect on excitons at all in the dilute limit.

Our study provides strong evidence that the two geometries of the oxygen interstitial would result in one (octahedral) or more (tetrahedral) electronic states midway into the bulk band gap. Their low enthalpy of formation indicates they could produce strong emission lines in photoluminescence in defective samples grown in copper-poor conditions, which would be suppressed under copper-rich growth conditions. Their energies are also sensitive to the charge state of the defect, meaning they could be responsible for multiple emission lines. Further analysis of these defects with excited-state methods could be fruitful.

It is possible that the $V_{\text{Cu}}^{s;1}$ defect would produce a defect state in the band gap, and therefore a line in the photoluminescence, however the fact that the state only appears under HSE means it could be a non-physical artefact of the XC-functional. If it were physical, it's consistently very low formation energy would make it a common defect, especially in samples grown in copper-poor condi-

tions. On the other hand, the defect state only supports one electron per defect, as opposed to the two (spin up and spin down) electrons supported by each level from the oxygen interstitials, so the $V_{\text{Cu}}^{s;1}$ line may be suppressed.

It is also possible that the copper interstitials would produce defect states in the band gap. The effect of the defect is too long range to be properly converged in the $3 \times 3 \times 3$ PBE supercell, so it is difficult to say whether the half-occupied band is a perturbation of the CBM or a poorly localised defect state. The much stronger exchange treatment in HSE06 splits this band by spin and populates fully one of the spin channels, but hybrid functionals are known to do poorly with metal-like states such as this one [47]. Given how strongly these defects interact with neighbouring defects, it is also hard to say whether this splitting would decay to zero in the dilute limit. If the defect did have a state in the band gap, it is safe to say it would lie near the bottom of the conduction band and produce photoemission of energy similar to the band gap energy, ~ 2 eV. The much higher formation enthalpy of the tetrahedral site would indicate that the octahedral interstitial would be significantly brighter in PL.

Despite being well under-converged in supercell size in this study, the HSE results indicate it is possible that the copper anti-site could introduce a defect state into the band gap in the dilute limit. Nevertheless, its prohibitively high formation energy would prevent it from contributing any signal to the photoluminescence spectrum.

Unfortunately, more than 5 possible photoluminescent states have emerged from this study, so we cannot conclude definitively on which PL lines are due to which defects. Six states come from each oxygen interstitial in charge states 0, -1, and -2; potentially two, close in energy, come from the copper interstitials; and potentially

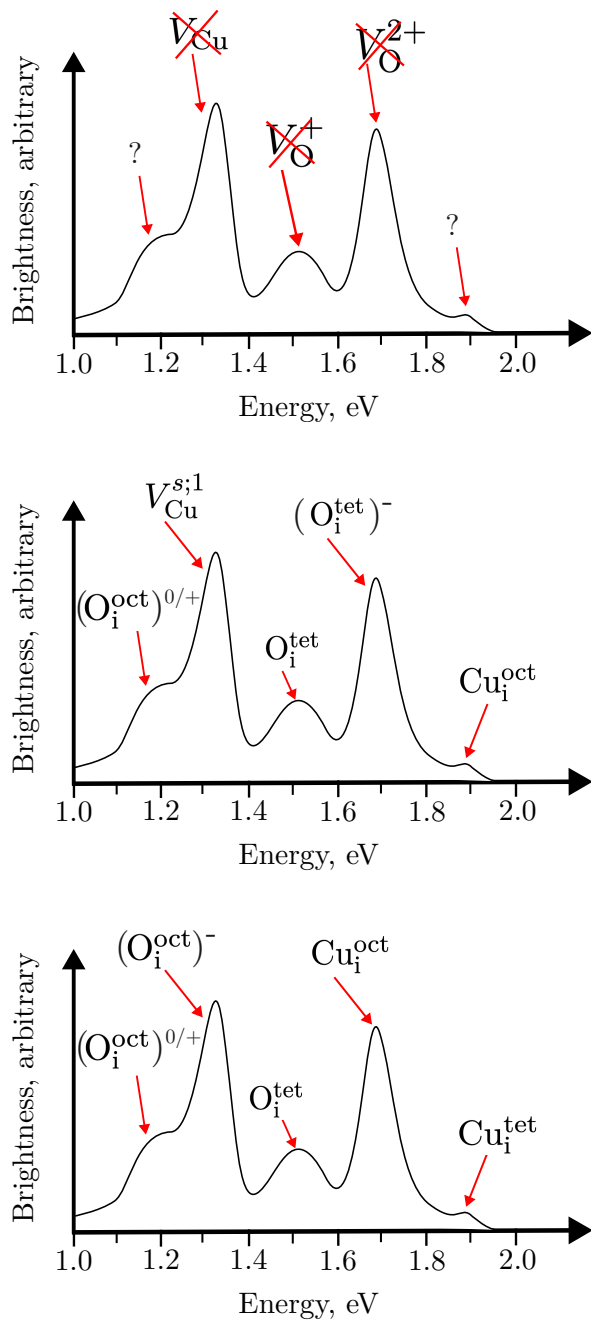


Figure 10: Sketches of all the commonly observed lines in photoluminescence experiments on Cu_2O . Top: the unsupported line assignments removed; middle: a possible reassignment of the PL lines based on the findings in this work; bottom: another possible assignment of the PL lines.

one comes from $\text{V}_{\text{Cu}}^{s;1}$. Given the trouble DFT has with accurately predicting band gaps, it is hard to directly relate the energy of the defect state to that of a photoemission line, especially given the additional error bar of ± 0.2 eV from the lack of spin-orbit coupling. Even if we were to extend the PBE and HSE gap artificially to their experimental values, it is not clear whether we should keep the defect states at their gap above the VBM, at their gap below the CBM, or something else entirely. Having said that, PBE and HSE both seem to agree roughly on the fractional position of a given defect state within the respective gaps, so we use the approximate energy ordering of the states to suggest several plausible PL line assignments.

The lowest energies from this set are $(\text{O}_i^{\text{oct}})^{0/+}$ and $\text{V}_{\text{Cu}}^{s;1}$, so we are encouraged to assign the 1.2 eV and 1.35 eV lines to some of these states. These two lines also commonly seen together, which could be because $\text{V}_{\text{Cu}}^{s;1}$ and O_i^{oct} both have a lower formation energy under oxygen rich conditions, or because they are due to two or more charge states of O_i^{oct} . This second hypothesis is also supported by the fact that the two lines are separated by ~ 0.1 eV, which is also how much the defect level rises by from $(\text{O}_i^{\text{oct}})^{0/+}$ to $(\text{O}_i^{\text{oct}})^-$. For the same reason, it is also possible that the line at 1.5 eV is due to $(\text{O}_i^{\text{oct}})^{2-}$.

The next-lowest defect state energy is from O_i^{tet} , so it could be the cause of the 1.5 or 1.7 eV lines. Given the 0.2 eV rise in this defect level that results from adding electrons, it is also possible that the 1.7 and 1.9 eV lines are due to $(\text{O}_i^{\text{tet}})^-$ and $(\text{O}_i^{\text{tet}})^{2-}$. Under the hypothesis that all the lines are due to various charge states of the two geometries of oxygen interstitials, it is not clear what growth conditions could cause such varying concentrations of O_i geometries and charges. The influence of growth conditions is easier to explain if we assign some of the high energy lines (1.7 and 1.9 eV) to the copper interstitials. Since, under PBE, they have very similar defect level energies, it is even possible that the two geometries contribute to the same PL line.

Figure 10 shows 2 possible peak re-assignments based on the evidence present in this study. As stated above, the results of this study are not sufficient to make concrete re-assignments of the PL lines to defect sites. Much stronger conclusions could be drawn from excited state calculations (GW or BSE) starting with HSE-DFT, as this would give quantitative emission spectra, with more accurate excitation energies attenuated by optical matrix elements.

6 Conclusion

In this work we have carried out a thorough *ab initio* investigation into the possible origins of the below-gap photoluminescence lines for Cu₂O. Indeed, the level of detail necessary to be certain of the stability of defect states in such a strongly correlated material, including the analysis of the complete band structure across varying supercell size and XC-functional, constitutes a new methodology in the study of defects within DFT. Using this new methodology, we have shown that there is no evidence within DFT that the simple copper and oxygen vacancies produce defect states in the band gap. Therefore, either there is some physics governing the behaviour of these defects that PBE- or HSE-DFT is not capturing, or they are not responsible for any PL lines, contrary to literature. We have shown that the oxygen interstitials consistently produce defect states within the band gap, across all levels of theory and supercell sizes studied, so it is likely that they are responsible for at least some of the PL lines. It is not clear whether, according to DFT, the copper interstitials, the first split copper vacancy, or the copper anti-site would produce defect states in the band gap, problems that could be solved with the ability to perform PBE calculations in $4 \times 4 \times 4$ supercells or HSE calculations in $3 \times 3 \times 3$ supercells. This method cannot quantitatively predict the PL emission energies, so it is difficult to make a strong reassignment of the lines based on the findings here. We offer several plausible reassessments of the PL lines based on oxygen interstitials, copper per interstitials, and the first split copper vacancy. Future work may be able to quantitatively predict the PL spectrum from each defect with excited state methods such as GW and BSE. The findings in this study are essential for the growth of high quality synthetic cuprous oxide, supporting the development of scalable technologies based of Rydberg excitons.

7 Acknowledgements

We would like to thank Stefan Scheel and Nikitas Gi-dopoulos for their generous theoretical discussions.

References

- [1] J Bloem. Discussion of some optical and electrical properties of cu₂o. *Philips Research Reports*, 13:167–193, 1958.
- [2] JH Apfel and AM Portis. Exciton-induced photoconductivity in cu₂o. *Journal of Physics and Chemistry of Solids*, 15(1-2):33–38, 1960.
- [3] K Akimoto, S Ishizuka, M Yanagita, Y Nawa, Goutam K Paul, and T Sakurai. Thin film deposition of cu₂o and application for solar cells. *Solar energy*, 80(6):715–722, 2006.
- [4] Lung-Chien Chen. Review of preparation and optoelectronic characteristics of cu₂o-based solar cells with nanostructure. *Materials Science in Semiconductor Processing*, 16(5):1172–1185, 2013.
- [5] T Kazimierczuk, D. Fröhlich, S. Scheel, H. Stolz, and M. Bayer. Giant Rydberg excitons in the copper oxide Cu₂O. *Nature*, 514(7522):343–347, 2014. URL: <https://www.nature.com/articles/nature13832>, doi:10.1038/nature13832.
- [6] J Heckötter, M Aßmann, and M Bayer. Rydberg excitons and quantum sensing. *MRS Bulletin*, 49(9):948–957, 2024.
- [7] Konstantinos Orfanakis, Sai Kiran Rajendran, Valentin Walther, Thomas Volz, Thomas Pohl, and Hamid Ohadi. Rydberg exciton–polaritons in a cu₂o microcavity. *Nature Materials*, 21(7):767–772, 2022.
- [8] Jon D. Pritchett, Liam A. P. Gallagher, Alistair Brewin, Horatio Q. X. Wong, Wolfgang Langbein, Stephen A. Lynch, C. Stuart Adams, and Matthew P. A. Jones. Giant microwave–optical Kerr nonlinearity via Rydberg excitons in cuprous oxide. *APL Photonics*, 9(3):031303, 03 2024. doi:10.1063/5.0192710.
- [9] Alistair Brewin, Liam AP Gallagher, Jonathan D Pritchett, Horatio QX Wong, Robert M Potvliege, Stewart J Clark, and Matthew PA Jones. Microwave-optical spectroscopy of Rydberg excitons in the ultrastrong driving regime. *New Journal of Physics*, 26(11):113018, 2024.
- [10] J. Heckötter, D. Janas, R. Schwartz, M. Aßmann, and M. Bayer. Experimental limitation in extending the exciton series in Cu₂O towards higher principal quantum numbers. *Phys. Rev. B*, 101:235207, Jun 2020. URL: <https://link.aps.org/doi/10.1103/PhysRevB.101.235207>, doi:10.1103/PhysRevB.101.235207.

[11] Stephen A. Lynch, Chris Hodges, Soumen Mandal, Wolfgang Langbein, Ravi P. Singh, Liam A. P. Gallagher, Jon D. Pritchett, Danielle Pizzey, Joshua P. Rogers, Charles S. Adams, and Matthew P. A. Jones. Rydberg excitons in synthetic cuprous oxide Cu₂O. *Phys. Rev. Mater.*, 5:084602, Aug 2021. URL: <https://link.aps.org/doi/10.1103/PhysRevMaterials.5.084602>, doi:10.1103/PhysRevMaterials.5.084602.

[12] Sjard Ole Krüger, Heinrich Stolz, and Stefan Scheel. Interaction of charged impurities and Rydberg excitons in cuprous oxide. *Phys. Rev. B*, 101:235204, Jun 2020. URL: <https://link.aps.org/doi/10.1103/PhysRevB.101.235204>, doi:10.1103/PhysRevB.101.235204.

[13] Martin Bergen, Valentin Walther, Binodbihari Panda, Mariam Harati, Simon Siegeroth, Julian Heckötter, and Marc Aßmann. Taming charged defects: Large scale purification in semiconductors using Rydberg excitons. *arXiv preprint arXiv:2310.11726*, 2023.

[14] Marijn A. M. Versteegh, Stephan Steinhauer, Josip Bajo, Thomas Lettner, Ariadna Soro, Alena Romanova, Samuel Gyger, Lucas Schweickert, André Mysyrowicz, and Val Zwiller. Giant Rydberg excitons in Cu₂O probed by photoluminescence excitation spectroscopy. *Phys. Rev. B*, 104:245206, Dec 2021. URL: <https://link.aps.org/doi/10.1103/PhysRevB.104.245206>, doi:10.1103/PhysRevB.104.245206.

[15] Stephan Steinhauer, Marijn AM Versteegh, Samuel Gyger, Ali W Elshaari, Birgit Kunert, André Mysyrowicz, and Val Zwiller. Rydberg excitons in Cu₂O microcrystals grown on a silicon platform. *Communications Materials*, 1(1):11, 2020.

[16] AV Mazanik, AI Kulak, EA Bondarenko, OV Korolik, NS Mahon, and EA Streltsov. Strong room temperature exciton photoluminescence in electrochemically deposited Cu₂O films. *Journal of Luminescence*, 251:119227, 2022.

[17] Kelvin B Chang, Laszlo Frazer, Johanna J Schwartz, John B Ketterson, and Kenneth R Poeppelmeier. Removal of copper vacancies in cuprous oxide single crystals grown by the floating zone method. *Crystal growth & design*, 13(11):4914–4922, 2013.

[18] Laszlo Frazer, Erik J Lenferink, Kelvin B Chang, Kenneth R Poeppelmeier, Nathaniel P Stern, and John B Ketterson. Evaluation of defects in cuprous oxide through exciton luminescence imaging. *Journal of Luminescence*, 159:294–302, 2015.

[19] Laszlo Frazer, Kelvin B Chang, Richard D Schaller, Kenneth R Poeppelmeier, and John B Ketterson. Vacancy relaxation in cuprous oxide (Cu_{2-x}O). *Journal of Luminescence*, 183:281–290, 2017.

[20] Sandhya Koirala, Nobuko Naka, and Koichiro Tanaka. Correlated lifetimes of free paraexcitons and excitons trapped at oxygen vacancies in cuprous oxide. *Journal of luminescence*, 134:524–527, 2013.

[21] Junqiang Li, Zenxia Mei, Daqian Ye, Huili Liang, Lishu Liu, Yaoping Liu, Augustinas Galeckas, Andrej Yu Kuznetsov, and Xiaolong Du. Engineering of optically defect free Cu₂O enabling exciton luminescence at room temperature. *Optical Materials Express*, 3(12):2072–2077, 2013.

[22] Takayuki Ito and Taizo Masumi. Detailed examination of relaxation processes of excitons in photoluminescence spectra of Cu₂O. *Journal of the Physical Society of Japan*, 66(7):2185–2193, 1997.

[23] Francesco Biccari. *Defects and doping in Cu₂O*. PhD thesis, Sapienza, Universita di Roma, 2012.

[24] Hannes Raebiger, Stephan Lany, and Alex Zunger. Origins of the p-type nature and cation deficiency in Cu₂O and related materials. *Physical Review B—Condensed Matter and Materials Physics*, 76(4):045209, 2007.

[25] Aloysius Soon, Xiang-Yuan Cui, Bernard Delley, Su-Huai Wei, and Catherine Stampfl. Native defect-induced multifarious magnetism in nonstoichiometric cuprous oxide: First-principles study of bulk and surface properties of Cu_{2-δ}O. *Physical Review B—Condensed Matter and Materials Physics*, 79(3):035205, 2009.

[26] David O Scanlon, Benjamin J Morgan, Graeme W Watson, and Aron Walsh. Acceptor levels in p-type Cu₂O: rationalizing theory and experiment. *Physical review letters*, 103(9):096405, 2009.

[27] Leah Y Isseroff and Emily A Carter. Electronic structure of pure and doped cuprous oxide with copper vacancies: suppression of trap states. *Chemistry of Materials*, 25(3):253–265, 2013.

[28] Eliseo Ruiz, Santiago Alvarez, Pere Alemany, and Robert A Evarestov. Electronic structure and properties of cu₂o. *Physical Review B*, 56(12):7189, 1997.

[29] Fabien Bruneval, Nathalie Vast, Lucia Reining, M Izquierdo, F Sirotti, and N Barrett. Exchange and correlation effects in electronic excitations of cu₂o. *Physical review letters*, 97(26):267601, 2006.

[30] Adib J Samin and James C Petrosky. An analysis of point defects in znte using density functional theory calculations. *Journal of Alloys and Compounds*, 921:166017, 2022.

[31] Yang Li, Guokai Hao, Jianyu Bai, Tingting Sui, Lieming Wei, Xun Sun, Xian Zhao, Mingxia Xu, and Baoan Liu. Structural and electronic properties and optical absorption of oxygen vacancy cluster defects in kdp crystals: hybrid density functional theory investigation. *CrystEngComm*, 25(19):2959–2965, 2023.

[32] Thomas Smith, Samuel Moxon, S Tse Joshua, Jonathan M Skelton, David J Cooke, Lisa J Gillie, E Lora da Silva, Robert M Harker, Mark T Storr, Stephen C Parker, et al. Structural dynamics of schottky and frenkel defects in ceo₂: a density-functional theory study. *Journal of Physics: Energy*, 5(2):025004, 2023.

[33] Xuefei Liu, Yuefei Zhang, Wentao Wang, Yuanzheng Chen, Wenjun Xiao, Tianyun Liu, Zhen Zhong, Zijiang Luo, Zhao Ding, and Zhaofu Zhang. Transition metal and n doping on alp monolayers for bifunctional oxygen electrocatalysts: density functional theory study assisted by machine learning description. *ACS Applied Materials & Interfaces*, 14(1):1249–1259, 2021.

[34] Samuel T Murphy. A point defect model for yba₂cu₃o₇ from density functional theory. *Journal of Physics Communications*, 4(11):115003, 2020.

[35] Yağmur Aksu Korkmaz, Ceyhun Bulutay, and Cem Sevik. Defect states in monolayer hexagonal bn: A comparative dft and dft-1/2 study. *Physica B: Condensed Matter*, 584:411959, 2020.

[36] Ina Østrøm, Md Anower Hossain, Patrick A Burr, Judy N Hart, and Bram Hoex. Designing 3d metal oxides: selecting optimal density functionals for strongly correlated materials. *Physical Chemistry Chemical Physics*, 24(23):14119–14139, 2022.

[37] John P Perdew, Kieron Burke, and Matthias Ernzerhof. Generalized gradient approximation made simple. *Physical review letters*, 77(18):3865, 1996.

[38] Jochen Heyd, Gustavo E Scuseria, and Matthias Ernzerhof. Hybrid functionals based on a screened coulomb potential. *The Journal of chemical physics*, 118(18):8207–8215, 2003.

[39] Jochen Heyd and Gustavo E Scuseria. Efficient hybrid density functional calculations in solids: Assessment of the heyd–scuseria–ernzerhof screened coulomb hybrid functional. *The Journal of chemical physics*, 121(3):1187–1192, 2004.

[40] Stewart J Clark, Matthew D Segall, Chris J Pickard, Phil J Hasnip, Matt IJ Probert, Keith Refson, and Mike C Payne. First principles methods using castep. *Zeitschrift für kristallographie-crystalline materials*, 220(5-6):567–570, 2005.

[41] Juan E Peralta, Jochen Heyd, Gustavo E Scuseria, and Richard L Martin. Spin-orbit splittings and energy band gaps calculated with the heyd–scuseria–ernzerhof screened hybrid functional. *Physical Review B—Condensed Matter and Materials Physics*, 74(7):073101, 2006.

[42] Frank Schweiner, Jörg Main, Günter Wunner, and Christoph Uihlein. Even exciton series in cu₂o. *Physical Review B*, 95(19):195201, 2017.

[43] Nanchen Dongfang, Yasmine S Al-Hamdan, and Marcella Iannuzzi. Understanding the role of oxygen-vacancy defects in cu₂o (111) from first-principle calculations. *Electronic Structure*, 5(3):035001, 2023.

[44] Michael Nolan and Simon D. Elliott. The p-type conduction mechanism in cu₂o: a first principles study. *Physical Chemistry Chemical Physics*, 8(45):5350, 2006. URL: <https://xlink.rsc.org/?DOI=b611969g>, doi:10.1039/b611969g.

[45] HA Al-Jawhari. A review of recent advances in transparent p-type cu₂o-based thin film transistors. *Materials Science in Semiconductor Processing*, 40:241–252, 2015.

[46] Takayuki Ito, Hiroyuki Yamaguchi, Katsuya Okabe, and Taizo Masumi. Single-crystal growth and characterization of cu₂o and cuo. *Journal of materials science*, 33:3555–3566, 1998.

[47] Weiwei Gao, Tesfaye A Abtew, Tianyi Cai, Yi-Yang Sun, Shengbai Zhang, and Peihong Zhang. On the applicability of hybrid functionals for predicting fundamental properties of metals. *Solid State Communications*, 234:10–13, 2016.